Longitudinal spin current induced by a temperature gradient in a ferromagnetic insulator

S. R. Etesami,[1,2] L. Chotorlishvili,[2] A. Sukhov,[2] and J. Berakdar[2]
[1]*Max-Planck-Institut für Mikrostrukturphysik, 06120 Halle, Germany*
[2]*Institut für Physik, Martin-Luther-Universität Halle-Wittenberg, 06120 Halle, Germany*
(Received 29 January 2014; revised manuscript received 25 June 2014; published 11 July 2014)

Based on the solution of the stochastic Landau-Lifshitz-Gilbert equation discretized for a ferromagnetic chain subject to a uniform temperature gradient, we present a detailed numerical study of the spin dynamics with a particular focus on finite-size effects. We calculate and analyze the net longitudinal spin current for various temperature gradients, chain lengths, and external static magnetic fields. In addition, we model an interface formed by a nonuniformly magnetized finite-size ferromagnetic insulator and a normal metal and inspect the effects of enhanced Gilbert damping on the formation of the space-dependent spin current within the chain. One aim of this study is the inspection of the spin-Seebeck effect beyond the linear response regime. We find that within our model the microscopic mechanism of the spin-Seebeck current is the magnon accumulation effect quantified in terms of the exchange spin torque. According to our results, this effect drives the spin-Seebeck current even in the absence of a deviation between the magnon and phonon temperature profiles. The influence of the dipole-dipole interaction and domain formation on the spin current is exposed and discussed. Our theoretical findings are in line with the recently observed experimental results by Agrawal *et al.* [Phys. Rev. Lett. **109**, 107204 (2012)].

DOI: 10.1103/PhysRevB.90.014410 PACS number(s): 85.75.−d, 73.50.Lw, 72.25.Pn, 71.36.+c

I. INTRODUCTION

Thermal magnetic and electric effects have a long history and are the basis for a wide range of contemporary devices. Research activities revived substantially upon the experimental demonstration of the correlation between an applied temperature gradient and the observed spin dynamics, including a spin current along the temperature gradient in an open-circuit magnetic sample, the so-called spin-Seebeck effect (SSE) [1]. Meanwhile, an impressive body of work has accumulated on thermally induced spin and spin-dependent currents [1–11] (for a dedicated discussion, we refer to the topical review [12]). The SSE was observed not only in metallic ferromagnets (FMs) like Co_2MnSi or semiconducting FMs, e.g., GaMnAs [4], but also in magnetic insulators $LaY_2Fe_5O_{12}$ [5] and (Mn, Ze)Fe_2O_4 [7]. The Seebeck effect is usually quantified by the Seebeck coefficient S which is defined, in a linear response manner, as the ratio of the generated electric voltage ΔV to the temperature difference ΔT: $S = -\frac{\Delta V}{\Delta T}$. The magnitude of the Seebeck coefficient S depends on the scattering rate and the density of electron states at the Fermi level, and thus it is a material-dependent variable. In the case of SSE, the spin voltage is formally determined by $\mu_\uparrow - \mu_\downarrow$, where $\mu_{\downarrow(\uparrow)}$ are the electrochemical potentials for spin-up and spin-down electrons, respectively. The density of states and the scattering rate for spin-up and spin-down electrons are commonly different, which results in various Seebeck constants for the two spin channels. In a metallic magnet subjected to a temperature gradient, one may think of the electrons in different spin channels to generate different driving forces, leading to a spin voltage that induces a nonzero spin current. When a magnetic insulator is in contact with a normal metal (NM) and the system is subjected to a thermal gradient, the total spin current flowing through the interface is a sum of two oppositely directed currents. The current emitted from the FM into the NM is commonly identified as a spin-pumping current I_{sp} and originates from the thermally activated magnetization dynamics in the FM, while the other current I_{fl} is associated with the thermal fluctuations in the NM and is known as spin torque [13]. The competition between the spin-pump and the spin-torque currents defines the direction of the total spin current which is proportional to the thermal gradient applied to the system. The theory of the magnon-driven SSE [5] presupposes that the magnon temperature follows the phonon temperature profile and in a linear response approximation provides a good agreement with experiments.

In a recent study [14] the theory of the magnon-driven SSE was extended beyond the linear response approximation. In particular, it was shown that the nonlinearity leads to a saturation of the total spin current and nonlinear effects become dominant when the inequality $H_0/T_F^m < k_B/(M_s V)$ holds, where H_0 is the constant magnetic field applied to the system, T_F^m is the magnon temperature, M_s is the saturation magnetization and V is the volume of the sample. The macrospin formulation of the stochastic Landau-Lifshitz-Gilbert (LLG) equation and the Fokker-Planck approach utilized in Ref. [14] is inappropriate for nonuniformly magnetized samples with characteristic lengths exceeding several 10 nm. Beyond the macrospin formulation the SSE effect for nonuniformly magnetized samples can be described by introducing a local magnetization vector [15] $\vec{m}(\vec{r},t)$. In this case, however, the corresponding Fokker-Planck equation turns into an integro-differential equation and can only be solved after a linearization [16]. Recently [17], the longitudinal SSE was studied in a NM-FM-NM sandwich structure in the case of a nonuniform magnetization profile. The linear regime, however, cannot totally embrace nontrivial and affluent physics of the SSE.

The paper is organized as follows. Section II defines the context of the current study and the relevance of the predictions for experiments. After setting the theory framework in Sec. III, in Sec. IV we introduce a definition of the spin current in a chain of interacting classical magnetic moments. In Sec. V we

analyze the numerical results, with emphasis on the role of the thermal bias magnitude, finite-size effects, the dependence of the spin current on an external magnetic field, and the type of boundary conditions. Particular attention is devoted to interface effects (Sec. VI) and the mechanisms of the formation of the spin current (Sec. VII). We finally consider the effects of the dipole-dipole interaction and magnetic domain formation on the spin current in Sec. VIII and conclude our paper in Sec. IX.

II. MOTIVATION AND FORMULATION OF THE PROBLEM

The spin current in magnetic insulators under a thermal gradient is mediated by thermally excited magnons. Thus, the concept of "magnon temperature" is of key importance for the problem of a thermally activated spin current. An external thermal bias applied to the system couples to the phonon subsystem that reaches a steady state swiftly while the magnons relax on a longer time scale (see [6] and references therein). Therefore, the formation of the magnon temperature profile proceeds for the already established phonon temperature profile. Furthermore, as long as anharmonic phononic effects are subsidiary, the creation of localized phonon excitations with higher density of modes is not relevant as well. As a result, one expects a linear phonon temperature profile and no variations of the temperature gradient across the system when the thermal bias is applied to the edges of a homogeneous phononic system. In contrast, the magnon temperature profile formed on a longer time scale is not necessarily linear because of the inherent nonlinearity of LLG equation. Therefore, in general, we expect to observe magnon accumulation phenomena.

This observation is important insofar as the formation of the thermally activated spin current was brought in connection with the existence of a temperature difference between the phonon and the magnon subsystems. Recent studies based on the macrospin approach valid for thin samples in the linear response approximation [6] and in the nonlinear regime [14] supported this point of view. In both cases the obtained analytical expressions for the spin current are proportional to the difference between the phonon and the magnon temperatures. The results of recent experiments [18] demonstrate, however, that in the case of finite-width samples the situation is different. A nonzero spin current was observed even for the case when the magnon temperature profile coincides with the phonon temperature profile. Making use of an infrared camera the local phonon temperature in the sample was measured, and it was shown that the phonon temperature $T_L > T_n^{ph} > T_R$ along the sample varies almost linearly under a thermal bias applied as different temperatures T_L and T_R to the left and to the right edges of the sample, respectively. This implies that a theoretical description of the formation of thermally induced spin current in a finite-size magnetic sample has to go beyond the single macrospin model (as done here). The main purpose of the present project is to study the mechanisms of the formation of the thermally activated spin current in nonuniformly magnetized finite-size magnetic insulator materials. Here we demonstrate that the mechanism is based on the magnon accumulation effect. It is quantified in terms of a slight change of the magnetization profile: $\langle \Delta M_n^z \rangle = \langle M_n^z \rangle - \langle M_{0n}^z \rangle$, where $\langle M_n^z \rangle$ is the mean component of the nth magnetization moment for the case when a thermal bias $T_L > T_R$ is applied to the edges of the system and a phonon temperature profile $T_R < T_n^{ph} < T_L$ is formed. On the contrary, $\langle M_{0n}^z \rangle$ corresponds to the mean magnetization component in the absence of a thermal gradient $T_L = T_R = T$, however, for the same uniform temperature applied along the whole chain $T = T_n^{ph}$. The quantity $\langle \Delta M_n^z \rangle$ defines the magnon accumulation as a difference between two equilibrium magnetization profiles formed for the same phonon temperature, but with and without the temperature gradient. We prove the direct connection between the magnon accumulation effect and the exchange spin torque and demonstrate that the exchange spin torque drives the spin current. In view of the experimental evidence [18], we account for the linear phonon temperature profile in our calculations via the random fluctuating term added to the LLG equations.

III. THEORETICAL FRAMEWORK

For the description of the transversal magnetization dynamics we consider propagation of the normalized magnetization direction $\vec{m}(\vec{r},t)$ as governed by the LLG equation [19,20],

$$\frac{\partial \vec{m}}{\partial t} = -\gamma[\vec{m} \times \vec{H}^{\text{eff}}] + \alpha \left[\vec{m} \times \frac{\partial \vec{m}}{\partial t}\right] - \gamma[\vec{m} \times \vec{h}(\vec{r},t)], \quad (1)$$

where the deterministic effective field $\vec{H}^{\text{eff}} = -\frac{1}{M_S}\frac{\delta F}{\delta \vec{m}}$ derives from the free energy density F and is augmented by a Gaussian white-noise random field $h(\vec{r},t)$ with a space-dependent local intensity and autocorrelation function. α is the Gilbert damping, $\gamma = 1.76 \times 10^{11}$ 1/(Ts) is the gyromagnetic ratio, and M_S is the saturation magnetization. F reads

$$F = \frac{1}{V}\int \left[\frac{A}{2}|\vec{\nabla} m|^2 + E_a(\vec{m}) - \mu_0 M_S \vec{H}_0 \cdot \vec{m}\right] dV, \quad (2)$$

where $\vec{H}_0$ is the external constant magnetic field, $E_a(\vec{m})$ is the anisotropy energy density, A is the exchange stiffness, and V is the volume of the system. We employ a discretized version of the integro-differential equation (1) by defining N cells with a characteristic length $a = \sqrt{2A/\mu_0 M_s^2}$ of the exchange interaction between the magnetic moments. $a^3 = \Omega_0$ is the volume of the respective cell. Assuming negligible variations of $\vec{m}(\vec{r},t)$ over a small a, one introduces a magnetization vector $\vec{M}_n$ averaged over the nth cell $\vec{M}_n = \frac{M_S}{V}\int_{\Omega_0} \vec{m}(\vec{r},t) dV$ and the total energy density becomes

$$\varepsilon = -\vec{H}_0 \cdot \sum_n \vec{M}_n + \frac{K_1}{M_S^2}\sum_n \left[M_S^2 - \left(M_n^z\right)^2\right] - \frac{2A}{a^2 M_S^2}\sum_n \vec{M}_n \cdot \vec{M}_{n+1}, \quad (3)$$

where $\vec{H}_0$ is the external magnetic field and K_1 is the uniaxial anisotropy density with the easy axis $\vec{e}_z$. The effective magnetic

field acting on the nth magnetic moment reads

$$\vec{H}_n^{\rm eff} = -\frac{\partial \varepsilon}{\partial \vec{M}_n} = \vec{H}_0 + \frac{2K_1}{M_S^2} M_n^z \vec{e}_z + \frac{2A}{a^2 M_S^2}(\vec{M}_{n+1} + \vec{M}_{n-1}). \quad (4)$$

Thermal activation is introduced by adding to the total effective field a stochastic fluctuating magnetic field $\vec{h}_n(t)$ so that

$$\vec{H}_n^{\rm eff}(t) = \vec{H}_0 + \vec{H}_n^{\rm anis} + \vec{H}_n^{\rm exch} + \vec{h}_n(t). \quad (5)$$

Here $\vec{H}_n^{\rm anis}$ is the magnetic anisotropy field and $\vec{H}_n^{\rm exch}$ is the exchange field. The random field $\vec{h}_n(t)$ has a thermal origin and simulates the interaction of the magnetization with a thermal heat bath (cf. the review Ref. [21] and references therein). The site dependence of $\vec{h}_n(t)$ reflects the existence of the local nonuniform temperature profile. On the scale of the volume Ω_0 the heat bath is considered to be uniform for a constant temperature. The random field is characterized via the standard statistical properties of the correlation function,

$$\langle h_{ik}(t)\rangle = 0,$$
$$\langle h_{ik}(t) h_{jl}(t+\Delta t)\rangle = \frac{2k_B T_i \alpha_i}{\gamma M_S a^3}\delta_{ij}\delta_{kl}\delta(\Delta t). \quad (6)$$

i and j define the corresponding sites of the FM chain and k and l correspond to the Cartesian components of the random magnetic field, T_i and α_i are the site-dependent local temperature and the dimensionless Gilbert damping constant, respectively, and $k_B = 1.38 \times 10^{-23}$ J/K is the Boltzmann constant.

We note that the correlation function of the random magnetic field can be quantified in terms of the effective magnon temperature. However, in the absence of the spin-torque current and enhanced Gilbert damping, when only the spin-pumping current exists, the effective magnon temperature coincides with the phonon temperature [6]. Furthermore, it is not the effective magnon temperature, but the real magnon temperature formed in the system which is of a key interest. This temperature should be calculated self-consistently (as explained and done below) from the magnetization dynamics after the system reaches the equilibrium. As demonstrated in this work, the self-consistently calculated magnon temperature differs from the phonon temperature profile.

In what follows we employ for the numerical calculations the material parameters related to yttrium iron garnet (YIG), e.g., as tabulated in Ref. [6] (Table I). Explicitly, the exchange stiffness is $A \approx 10$ pJ/m, the saturation magnetization has a value of $4\pi M_S \approx 10^6$ A/m. The anisotropy strength K_1 can be derived from the estimate for the frequency $\omega_0 = \gamma 2K_1/M_S \approx 10 \times 10^9$ s^{-1} [6]. The size of the FM cell is estimated from $a = \sqrt{2A/\mu_0 M_s^2}$, yielding about 20 nm. The values of all relevant parameters (A, K_1, M_S, α) are taken at 0 K, which seems to be a good approximation in view of their weak temperature dependence in the range of the temperatures relevant here (0K–100 K) [22,23]. For a damping parameter we take the value $\alpha = 0.01$, which exceeds the actual YIG value [5,6]. This is done to optimize the numerical procedure in order to obtain reasonable calculation times. We note that although the quasiequilibrium is assured when tracking the magnetization trajectories on the time scale longer than the relaxation time, the increased α quantitatively alters the strength in the correlation function [Eq. (6)] and therefore indirectly has an impact on the values of the spin current.

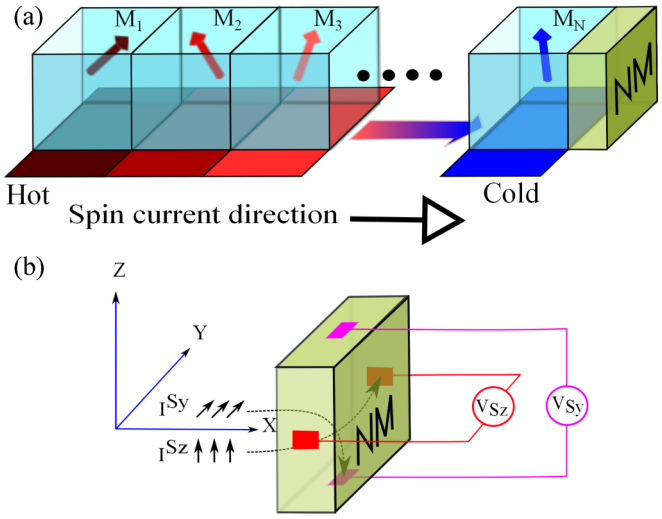

FIG. 1. (Color online) (a) Schematics of the FM chain considered in the calculations. (b) Suggested alignment for measurements.

We focus on a system representing a junction of a FM insulator and a NM which is schematically shown in Fig. 1. This illustration mimics the experimental setup for measuring the longitudinal SSE [24], even though the analysis performed here does not include all the aspects of the experimental setting. The direction of the magnetic moments in the equilibrium is parallel to the FM-NM interface. Experimentally, it was suggested to pick up the longitudinal spin current by means of the inverse spin Hall effect [24]. If it is so possible then, the electric field generated via the inverse spin Hall effect (ISHE) reads $\vec{\mathbf{E}} = D_0 \vec{\mathbf{I}}_s \times \vec{\sigma}$. Here $\vec{\mathbf{E}}$ denotes the electric field related to the ISHE, $\vec{\mathbf{I}}_s$ defines the spatial direction of the spin current, $\vec{\sigma}$ is the spin polarization of the electrons in the NM, and D_0 is a constant. We note, however, that our study is focused on the spin dynamics only and makes no statements on ISHE.

IV. DEFINITION OF THE SPIN CURRENT

For convenience we rewrite the Gilbert equation with the total energy density (3) in the form suggested in Ref. [17],

$$\frac{\partial \vec{S}_n}{\partial t} + \gamma\{\vec{S}_n \times [\vec{H}_n^{\rm eff}(t) - \vec{H}^{\rm ex}]\} + \frac{\alpha\gamma}{M_S}\left[\vec{S}_n \times \frac{\partial \vec{S}_n}{\partial t}\right] + \vec{\nabla}\cdot\vec{J}_n^{\vec{s}} = 0, \quad (7)$$

where $\vec{S}_n = -\vec{M}_n/\gamma$ and the expression for the spin-current density tensor reads

$$\vec{\nabla}\cdot\vec{J}_n^{\vec{s}} = \gamma[\vec{S}_n \times \vec{H}_n^{\rm ex}]. \quad (8)$$

Here

$$\vec{Q}_n = -\gamma[\vec{S}_n \times \vec{H}_n^{\rm ex}] \quad (9)$$

is the local exchange spin torque.

For the particular geometry (Fig. 1) the only nonzero components of the spin-current tensor are $I_n^{s_x}, I_n^{s_y}, I_n^{s_z}$. Taking into account Eqs. (4) and (7), we consider a discrete version of the gradient operator and for the components of the spin-current tensor $I_n^s = a^2 J_n^s$ we deduce

$$I_n^\alpha = I_0^\alpha - \frac{2Aa}{M_S^2} \sum_{m=1}^{n} M_m^\beta \left(M_{m-1}^\gamma + M_{m+1}^\gamma\right) \varepsilon_{\alpha\beta\gamma}, \qquad (10)$$

where $\varepsilon_{\alpha\beta\gamma}$ is the Levi-Civita antisymmetric tensor, Greek indexes define the current components, and the Latin ones denote sites of the FM chain. In what follows we utilize Eq. (10) for quantifying the spin current in the spin chain. We consider different temperature gradients applied to the system, taking into account the dependence of the magnon temperature on the phonon temperature profile [5]. Since the temperature in the chain is not uniform, we expect a rich dynamics of different magnetic moments $\vec{M}_n$. In this case only the nonuniform site-dependent spin current I_n can fulfill the equation (7). In order to prove this, we consider different configurations of magnetic fields for systems of different lengths. Modeling the interface effects between the FM insulator and the NM proceeds by invoking the concept of the enhanced Gilbert damping proposed in a recent study [25]. The increased damping constant in the LLG equation of the last magnetic moment describes losses of the spin current due to the interface effect. In order to evaluate the spin current flowing from the NM to the FM insulator we assume that the dynamics of the last spin in the insulator chain is influenced by the spin torque flowing from the NM to the magnetic insulator.

V. NUMERICAL RESULTS ON ISOLATED FERROMAGNETIC INSULATOR CHAIN

For the study of thermally activated magnetization dynamics we generate from 1000 to 10 000 random trajectories for each magnetic moment of the FM chain. All obtained observables are averaged over the statistical ensemble of stochastic trajectories. The number of realizations depends on the thermal gradient applied to the system. For long spin chains (up to 500 magnetic moments) the calculations are computationally intensive even for the optimized advanced numerical Heun method [26], which converges in quadratic mean to the solution of the LLG equation when interpreted in the sense of Stratonovich [27]. For the unit cell of the size 20 nm, the FM chain of 500 spins is equivalent to the magnetic insulator sample of the width around 10 μm. We make sure in our calculations that the magnetization dynamics is calculated on the large time scale exceeding the system's relaxation time, which can be approximated via $\tau_{\text{rel}} \approx M_S/(\gamma 2K_1\alpha) \approx$ 10 ns [28].

A. Role of the local temperature and local exchange spin torque

Prior to studying a realistic finite-size system, we consider a toy model of three coupled magnetic moments. Our aim is to better understand the role of the local temperature and the local exchange spin torque Q_n [Eq. (9)] in the formation of the spin current I_n. Considering Eqs. (8) and (9), we can utilize a recursive relation for the site-dependent spin current I_n and the local exchange spin torque $I_n = I_{n-1} + \frac{a^3}{\gamma} Q_n$ for different temperatures of the site in the middle of the chain above $T_2 > T_{\text{av}}$ and below $T_2 < T_{\text{av}}$. The mean temperature in the system is $T_{\text{av}} = (T_1 + T_2 + T_3)/3$. The calculations are performed for different values of the site temperatures. We find that the exchange spin torques Q_n related to magnetic moments M_n with a temperature above the mean temperature $T_n > T_{\text{av}}$ have a positive contribution to the spin current in contrast to the exchange spin torques Q_m of the on-average-"cold" magnetic moments with $T_m < T_{\text{av}}$. This finding hints at the existence of a maximum spin current in a finite chain of magnetic moments and/or strong temperature gradient. This means that the site-dependent spin current I_n increases if $Q_n > 0$ until the local site temperature drops below the mean temperature $T_n < T_{\text{av}}$, in which case the exchange spin torque becomes negative $Q_n < 0$ and the spin current decreases. In order to prove that the negative contribution in the spin current of the on-average-cold magnetic moments is not an artifact of the three magnetic moments only, we studied spatially extended spin chains as to simulate nonuniformly magnetized FM insulators. In the thermodynamic limit for a large number of magnetic moments $N \gg 1$ we expect to observe a formation of the equilibrium patterns in the spin-current profile corresponding to the zero exchange spin torque $Q_n = 0$ between nearest adjacent moments.

B. Longitudinal spin current

In Fig. 2 the dependence of distinct components of the spin current is plotted site-resolved. As inferred from the figure

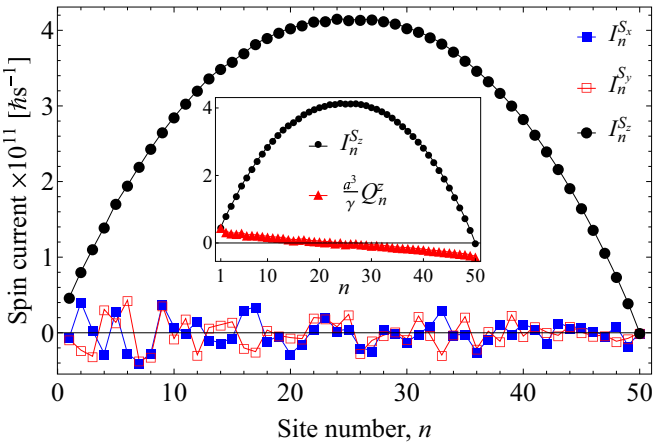

FIG. 2. (Color online) Different Cartesian components of the statistically averaged longitudinal spin current as a function of the site number. Numerical parameters are $\Delta T = 50$ K, $\alpha = 0.01$, and $H_0 = 0$ T. The temperature gradient is defined $\Delta T = T_1 - T_{50}$, where $T_1 = 50$ K. The only nonzero component of the spin current is $I_n^{S_z}$. Other two components $I_n^{S_x}$, $I_n^{S_y}$ are zero because of the uniaxial magnetic anisotropy field which preserves X0Y symmetry of the magnetization dynamics. The inset shows the z component of the statistically averaged spin current $I_n^{S_z}$ (blue solid circles) and the distribution of the exchange spin torque $\frac{a^3}{\gamma} Q_n^z$ (red solid triangles), both shown in a site-resolved manner. A direct correlation between the behavior of the spin current and the exchange spin torque can be observed: The change of the sign of the exchange spin torque matches exactly the maximum of the spin current.

the current is not uniformly distributed along the chain. In particular, the only nonzero component is $I_n^{S_z}$. This is due to the uniaxial anisotropy being aligned along the z axis, whereas the $I_n^{S_x}$ and $I_n^{S_y}$ components vanish on average due to symmetry considerations. Evidently, the spin current has a maximum in the middle of the chain. The site-dependent spin current is an aftermath of the nonuniform magnon temperature profile applied to the system. This effect was not observed in the single macrospin approximation and is only relevant for the nonuniformly magnetized finite-size magnetic insulator sample. In addition, one observes that the amplitude of the spin current increases with increasing the thermal gradient. This is predictably natural; less so, however, is the presence of a maximum of the spin current observed in the middle of the chain. We interpret this observation in terms of a collective cumulative averaged influence of the surrounding on the particular magnetic moment. For a linear temperature gradient, e.g., as in Fig. 2, we have $\Delta T = \frac{T_1 - T_N}{aN}$. Thus, half of the spine located at the sites $i < N/2$ possess temperatures above the mean temperature $T_1/2$, while the other half have temperatures below the mean temperature. Further, the main contributors to the total spin current are the hot magnetic moments with temperatures above the mean temperature $T_n > T_{\rm av}$ and with a positive exchange spin torque $Q_n > 0$, while magnetic moments with a temperature below the mean temperature $T_n < T_{\rm av}$, $Q_n < 0$ absorb the spin current and have a negative contribution in the total spin current. This nonequivalence of magnetic moments results in a maximum of the total spin current in the center of the chain. In what follows the magnetic moments with temperatures higher than the mean temperature in the chain are referred to as hot magnetic moments, while the magnetic moments with temperatures lower than $T_{\rm av}$ we refer to as cold magnetic moments (i.e., our reference temperature is $T_{\rm av}$). The idea we follow is that the hot magnetic moments cause the total spin current which is partly utilized for the activation of the cold magnetic moments. The inset of Fig. 2 illustrates this statement. The maximum of the spin current (solid circles) is observed in the vicinity of the sites where the exchange spin-torque term Q_n changes its sign from positive to negative (solid triangles), highlighting the role of the hot and cold magnetic moments in finite-size systems. To further affirm this, we consider two different temperature profiles—linear and exponential—with slightly shifted values of the mean temperature (Fig. 3). The dependence of the maximum spin current on the mean temperature is a quite robust effect and slight shifts of the mean temperature to the left lead to a certain shifting of the spin current's maximum. The effect of the nonuniform spin current passing through the finite-size magnetic insulator might be tested experimentally using the SSE setup in which the spin current's direction is parallel to the temperature gradient. One may employ the ISHE using a FM insulator covered by a stripe of paramagnetic metal, e.g., Pt at different sites (cf. Ref. [24]), albeit the chain must be small ($\lesssim 1$ μm).

C. Role of boundary conditions

To elaborate on the origin of the observed maximum of the spin current, we inspect the role of boundary conditions. In fact, in spite of employing different boundary conditions for the chain we observe the same effect [Fig. 4(a)], from which we can conclude that the effect of the cold and hot magnetic moments is inherent to the spin dynamics within the chain, which is independent from the particular choice of the boundary conditions. Furthermore, we model the situation with the extended region at the ends of the FM chain [Fig. 4(b)], in which the end temperatures are constant (i.e., one might imagine the heat reservoirs to have finite spatial extensions). Modeling the ends of the FM chain with zero temperature gradient by means of the LLG equations is certainly an approximation, which can be improved by employing the Landau-Lifshitz-Bloch equations reported in Ref. [12]. It captures, however, the main effects at relatively low temperatures: the flow of the spin current for the decaying spin density away from the $T = \text{const-}\Delta T$ interface and a nonzero integral spin current for the sites $0 < n < 50$ and $150 < n < 200$. As we see even in the fragments of the chain with a zero temperature gradient the spin current is not zero. The reason is that the formation of the spin-current profile is a collective many-body effect of the interacting magnetic moments. Therefore, the fragment of the chain with nonzero temperature gradient (sites $50 < n < 150$) has a significant influence on the formation of the spin-current profiles in the left and right regions of the chain where the temperature gradient vanishes.

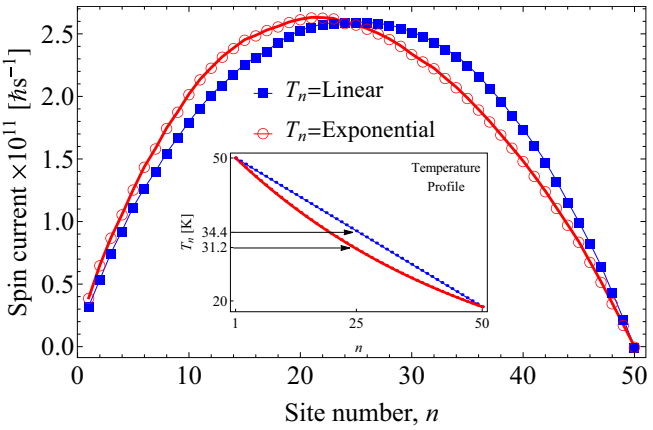

FIG. 3. (Color online) Z component of the statistically averaged spin current for the linear $\Delta T = T_1 - T_{50}$ and exponential $\Delta T(n) = 50\ \text{K}\, e^{-(n-1)/50}$ temperature gradients. The slight shift of the mean temperature to the left leads to a certain shifting of the maximum spin current to the left. The inset shows the temperature distribution in the FM chain.

D. Temperature dependence of the longitudinal spin current

Figure 5 shows the dependence of the z component of the averaged longitudinal spin current on the temperature gradient. Though the spin current within the chain is not uniform, the dependence of the local spin current detected in the middle of the chains $I_{26}(\Delta T)$ (inset of Fig. 5) is linear and the amplitude of the spin current increases with the temperature gradient. This result is consistent with the experimental facts (Refs. [4,5]) and our previous analytical estimations obtained via the single macrospin model [14]. Additionally, irrespective of the temperature bias, the $I_n^{S_z}$ dependence remains symmetric and no saturation of the spin current can be observed for this thickness.

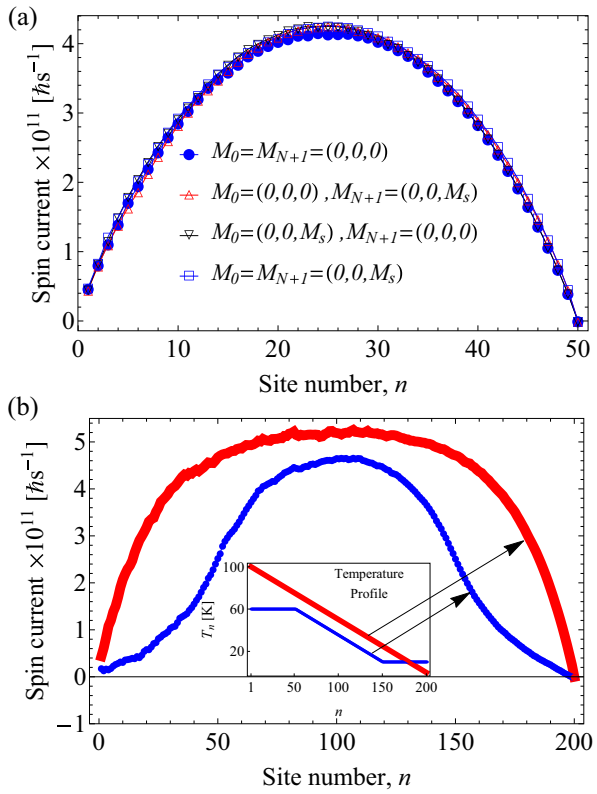

FIG. 4. (Color online) Effect of distinct boundary conditions. (a) Only the values of the first and last magnetic moments are kept constant, resulting in the same maximal spin current for the site number corresponding to the mean temperature of the system. The effect of the cold and hot magnetic moments is independent of the particular choice of the boundary conditions for the following numerical parameters: $\Delta T = 50$ K, $\alpha = 0.01$, and $H_0 = 0$ T. The temperature gradient is defined $\Delta T = T_1 - T_{50}$, where $T_1 = 50$ K. (b) Different temperature profiles are imposed on the boundaries: a linear temperature gradient (thick red curve) and a constant temperature for the ranges $0 < n < 50$ and $150 < n < 200$ (thin blue curve). For the fragments of the chain with zero temperature gradient the spin current is not zero, which results from the formation of the spin-current profile as a collective many-body effect of the interacting magnetic moments. Therefore, the fragment of the chain with nonzero temperature gradient (sites $50 < n < 150$) has a significant influence on the formation of the spin-current profiles in the left and right zero temperature gradient parts of the chain.

E. Finite-size effects

Finite-size effects are considered relevant for the experimental observations (e.g., Ref. [4]). In the thermodynamic limit $N \gg 1$ we expect the formation of equilibrium patterns in the spin-current profile corresponding to the zero exchange spin torque $Q_n = 0$ between nearest adjacent moments. To address this issue, the spin current for chains of different lengths is shown in Fig. 6. Obviously, in the case of $N = 500$ magnetic moments large pattern of the uniform spin current corresponding to the sites $50 < n < 450$ is observed. In order to understand such a behavior of the spin current for a large system size, we plotted the dependence on the site number of the exchange spin torque Q_n (Fig. 7). As we see, the exchange spin torque corresponding to the spin-current

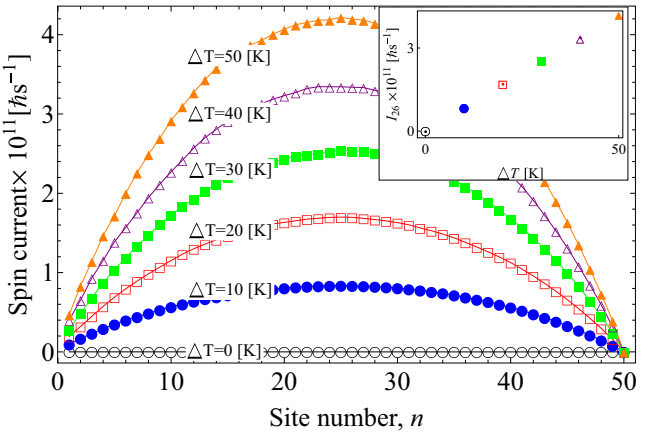

FIG. 5. (Color online) Dependence of the averaged spin current on the strength of the temperature gradient. Numerical parameters are $\alpha = 0.01$ and $H_0 = 0$ T. The temperature gradient is defined as $\Delta T = T_1 - T_{50}$, where $T_1 = 50$ K. The inset shows the averaged spin current for the 26th site. The maximum current increases with elevating the temperature gradient.

plateau is characterized by large fluctuations around zero value, while nonzero positive (negative) values of the exchange spin torque Q_n observed at the left (right) edges correspond to the nonmonotonic left and right wings of the spin-torque profile. One may try to interpret the observed results in terms of the so-called magnon relaxation length (MRL) $\lambda_m \approx 2\sqrt{(Dk_BT/\hbar^2)\tau_{mm}\tau_{mp}}$ (Refs. [5,6]), where D is the spin-wave stiffness constant and $\tau_{mm,mp}$ are the magnon-magnon and the magnon-phonon relaxation times, respectively. The MRL is a characteristic length which results from the solution of the heat-rate equation for the coupled magnon-phonon system [5]. The physical meaning of λ_m is an exponential drop of the space distribution of the local magnon temperature for the given external temperature gradient ΔT. In other words, although the externally applied temperature bias is kept constant, the thermal distribution for magnons is not necessarily linear. In

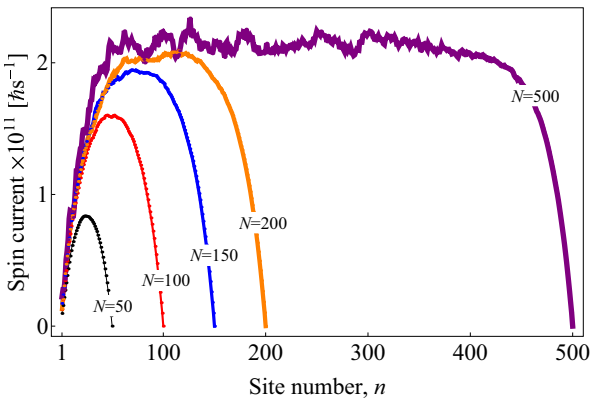

FIG. 6. (Color online) The dependence of the averaged spin current on the length of the FM chain. Numerical parameters are $\alpha = 0.01$ and $H_0 = 0$ K. The temperature gradient is linear and the maximum temperature is on the left-hand side of the chain ($T_1 = 100$ K). In all cases the per-site temperature gradient is $\Delta T/N = 0.2$ K.

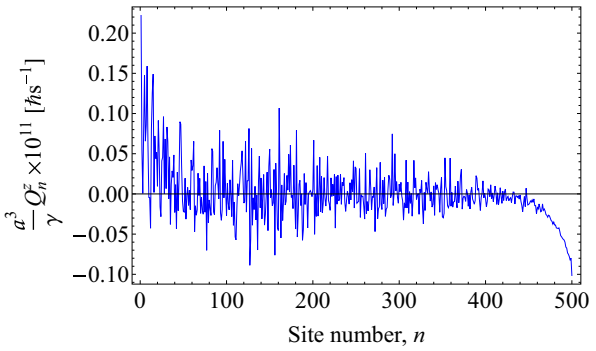

FIG. 7. (Color online) The dependence of the exchange spin torque on the site number. Numerical parameters are $\alpha = 0.01$ and $H_0 = 0$ K. The temperature gradient is linear and the maximum temperature is on the left-hand side of the chain ($T_1 = 100$ K). The per-site temperature gradient is $\Delta T/N = 0.2$ K. The exchange spin-torque profile consists of three parts. The positive part corresponds to the high-temperature domain and low-temperature domain corresponds to the negative exchange spin torque. In the middle of the chain, where the spin current is constant, the exchange spin torque fluctuates in the vicinity of the zero value.

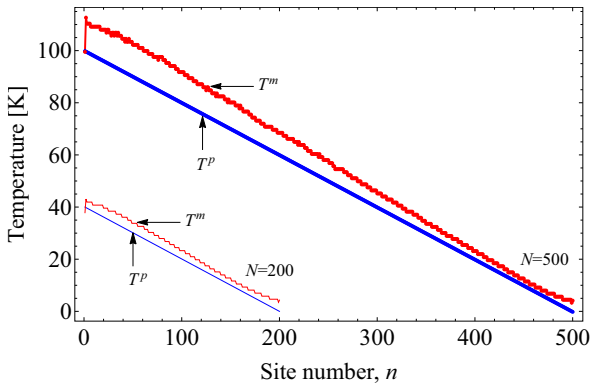

FIG. 8. (Color online) The magnon temperature profile (line) formed in the system. Numerical parameters are $\alpha = 0.01$ and $H_0 = 0$ K. The blue line corresponds to the applied linear phonon temperature profile. The maximum temperature on the left-hand side of the chain is ($T_1 = 100$ K). The per-site temperature gradient is $\Delta T/N = 0.2$ K. The maximal deviation between the phonon and magnon temperatures is observed only at the left edge of chain. The difference between temperatures gradually decreases and becomes almost zero for the sites with $n > 400$.

general, one may suggest a $\sinh(x)$-like spatial dependence [5] and a temperature dependence $\lambda_{\rm m}(T)$. Estimates of the MRL for the material parameters related to YIG (Supplemental Material of Ref. [5]) and $T_N = 0.2$ K yield the following: $\lambda_{\rm m} \approx 10\,\mu$m [29]. As seen from Fig. 6 the length starting from which the saturation of the spin current comes into play as long as the FM chain exceeds the length 20 nm $\times$ 100 $\approx 2\,\mu$m. However, we recall that MRL is a witness of the deviation between the magnon and the phonon temperature profiles. Therefore, for interpreting the nonmonotonic parts of the spin-current profile (Fig. 6) in terms of the MRL one has to prove the pronounced deviation between magnon and phonon temperatures at the boundaries. For further clarification we calculate the magnon temperature profile. This can be done self-consistently via the Langevin function $\langle M_n^z\rangle = L\left(\langle M_n^z\rangle H_n/k_B T_n^m\right)$. Here H_n^z is the z component of the local magnetic field which depends on the external magnetic field and the mean values of the adjacent magnetic moments $\langle M_{n-1}^z\rangle$, $\langle M_{n+1}^z\rangle$ [see Eq. (4)]. Figure 8 indicates that the magnon temperature profile follows the phonon temperature one. A pronounced deviation of the phonon and the magnon temperatures is observed only on the left edge of the chain and gradually decreases, becoming small on the MRL scale. Close to the end of the chain the temperature difference becomes almost zero. This means that the left nonmonotonic parts of the spin-current profile Fig. 6 can be interpreted in terms of nonequilibrium processes. Comparison of this result with the exchange spin-torque profile depicted in Fig. 7 convinces us that in this part of the spin chain the exchange spin torque is positive. For this reason, the spin current I_n increases with the site number n. The saturated plateau of the spin current shown in Fig. 6 corresponds to the zero exchange spin torque $Q_n = 0$ (cf. Fig. 7) and the decay of the spin-Seebeck current I_n at the right edge corresponds to the negative spin exchange torque $Q_n < 0$. Therefore, for the formation of the convex spin-current profile the key issue is not the difference between magnon and phonon temperatures. This is relatively small. In fact, the key element is the magnon temperature profile. The existence of the hot (cold) magnetic moments with the local magnon temperature above (below) the mean magnon temperature generates the spin current. This difference in the local magnon temperature of the different magnetic moments drives the spin current in the chain. On the other hand, any measurement of the spin current done in the vicinity of the right edge of the current profile will demonstrate a nonvanishing spin current in the absence of the deviation between the magnon and phonon temperature profiles. This may serve as an explanation of the recent experiment [18], where a nonvanishing spin current was observed in the absence of the deviation between the magnon and the phonon temperature profiles. We note that zero values of the spin current shown in Fig. 6 is an artifact of the isolated magnetic insulator chain. Real measurements of the spin currents usually involve FM insulator/NM interfaces. As shown below, the interface effect described by an enhanced Gilbert damping and the spin torque lead to a nonzero spin current at the interfaces, which is actually measured in the experiment.

F. Role of the external magnetic field ($H_0 \neq 0$)

It follows from our calculations that the dependence of the longitudinal spin current on the magnetic field is not trivial. As in Sec. V D, we focus on the middle of the FM chain with $N = 50$ and the results for the spin current $I_{26}^{S_z}(H_0)$. Once the external static magnetic field is applied perpendicular to the FM chain and along the easy axis at the same time, we can suppress the spin current at elevated magnetic fields [Fig. 9(a)]. The threshold magnetic field is—as expected—the strength of the magnetocrystalline anisotropy field, i.e., $2K_1/M_{\rm S} \sim 0.056$ T. By applying magnetic fields much higher than 0.056 T, the magnetic moments are fully aligned along the field direction and hence the X, Y components of the magnetization required

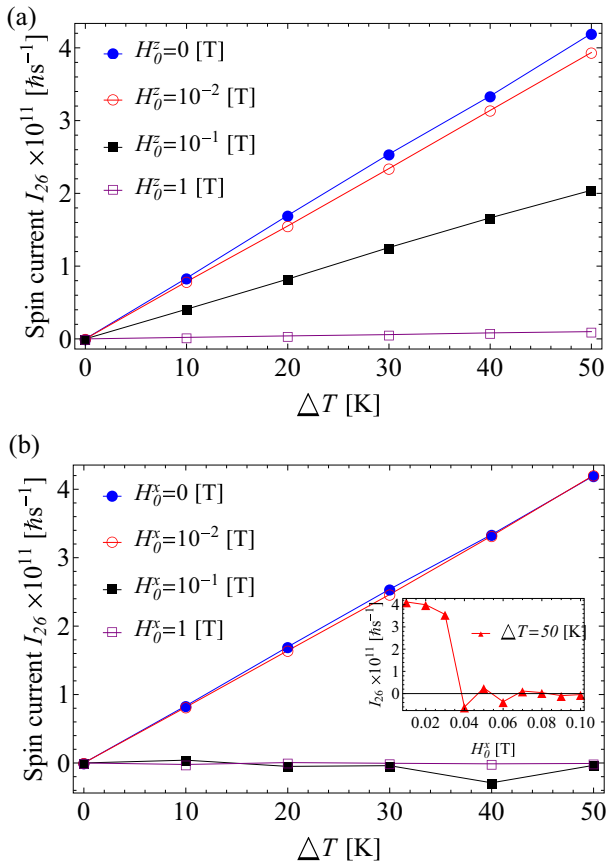

FIG. 9. (Color online) Effect of the external magnetic field applied parallel (a) to the easy axis and perpendicular (b) to the easy axis on the averaged spin current. Parameters of numerical calculations are $\Delta T = 50$ K, $\alpha = 0.01$, and $N = 50$. The temperature gradient is linear and the maximum temperature is imposed on the left-hand side of the chain. The inset of (b) demonstrates the field dependence of the averaged spin current calculated for the central magnetic moment.

to form the Z component of the longitudinal averaged spin current vanish.

In the case of the magnetic field being applied perpendicularly to the easy axis, we observe a richer behavior [Fig. 9(b)]. In analogy with the situation observed in Fig. 9(a) there are no sizable changes for the $I_{26}(\Delta T)$ dependence at low static fields. This is the regime where the anisotropy field is dominant. In contrast to the H_0^z applied field, the spin current does not linearly depend on the strength of the field [inset of Fig. 9(b)], which is explained by the presence of different competing contributions in the total energy density and not a simple correction of the Z component of the anisotropy field illustrated in the previous figure. Surprisingly, the magnetic field oriented along the FM chain can also suppress the appearance of the spin current's profile. Also in this case the strong magnetic field destroys the formation of the magnetization gradient resulting from the applied temperature bias.

VI. INTERFACE EFFECTS

The experimental setup to detect the spin current might involve a NM adjacent to the spin-current generating substance, e.g., a FM insulator. This NM converts the injected spin current from the FM to an electric current via ISHE [1,5,30]. So it is of interest to see the effect of the adjacent NM on the generated spin current in the considered chain. Obviously, the main effects appear in the FM-NM interface. The interface effect can be divided into two parts, which is described in the following subsections.

A. Spin pumping and enhanced Gilbert damping

In *magnetic insulators*, charge dynamics is less relevant (in our model, anyway), and in some cases the dissipative losses associated with the magnetization dynamics are exceptionally low (e.g., in YIG [31] $\alpha = 6.7\times10^{-5}$). When a magnetic insulator is brought into contact with a *NM*, magnetization dynamics results in spin pumping, which in turn causes angular momentum being pumped to the NM. Because of this nonlocal interaction, the magnetization losses become enhanced [25].

If we consider the NM as a *perfect spin sink* which remains in equilibrium even though spins are pumped into it (which means there is a rapid spin relaxation and no backflow of spin currents to the magnetic insulator), the magnetization dynamics is described by the LLG equation with an additional torque originating from the FM-insulator/NM interfacial spin pumping [25],

$$\frac{\partial \vec{M}}{\partial t} = -\gamma[\vec{M}\times\vec{H}^{\rm eff}] + \frac{\alpha}{M_{\rm S}}\left[\vec{M}\times\frac{\partial\vec{M}}{\partial t}\right] + \vec{\tau}^{\rm sp}, \quad (11)$$

where

$$\vec{\tau}^{\rm sp} = \frac{\gamma\hbar}{4\pi M_{\rm S}^2} g_{\rm eff}\delta(x-L)\left[\vec{M}\times\frac{\partial\vec{M}}{\partial t}\right], \quad (12)$$

where L is the position of the interface, e is the electron charge, and $g_{\rm eff}$ is the real part of the *effective* spin-mixing conductance. In the YIG-Pt bilayer the maximum measured effective spin-mixing conductance is $g_{\rm eff} = 4.8\times10^{20}$ m^{-2} [25]. In fact, if the spin-pumping torque should be completely described, one should add another torque containing the imaginary part of $g_{\rm eff}$ [32]. However, we omit this imaginary part here because it has been found to be too small at FM-NM interfaces [33].

The aforementioned spin-pumping torque concerns the cases that we characterized with $\vec{M}$. In our discrete model, which includes a chain of N ferromagnetic cells, we describe the above phenomena as

$$\frac{\partial \vec{M}_n}{\partial t} = -\gamma\left[\vec{M}_n\times\vec{H}_n^{\rm eff}\right] + \frac{\alpha}{M_{\rm S}}\left[\vec{M}_n\times\frac{\partial\vec{M}_n}{\partial t}\right] + \vec{\tau}_n^{\rm sp}, \quad (13)$$

where

$$\vec{\tau}_n^{\rm sp} = \frac{\gamma\hbar^2}{2ae^2M_{\rm S}^2} g_\perp\delta_{nN}\left[\vec{M}_n\times\frac{\partial\mathbf{M}_n}{\partial t}\right], \quad (14)$$

which means the spin pumping leads to an enhanced Gilbert damping in the last site,

$$\Delta\alpha = \frac{\gamma\hbar}{4\pi a M_s} g_{\rm eff}. \quad (15)$$

As already mentioned, the above-enhanced Gilbert damping could solely describe the interfacial effects as long as

we treat the adjacent NM as a perfect spin sink without any backflow of the spin current from the NM [17,25]. The latter is driven by the accumulated spins in the NM. If we model the NM as a perfect spin sink for the spin current, spin accumulation does not build up. This approximation is valid when the spin-flip relaxation time is very small and so it prevents any spin-accumulation buildup. So the spins injected by pumping decay and/or leave the interface sufficiently fast and there is no backscattering into the FM [13,34]. We note in passing that in a recent study concerning this phenomena it was shown that spin pumping (and so enhanced Gilbert damping) depends on the transverse mode number and in-plane wave vector [25].

B. Spin-transfer torque

It was independently proposed by Slonczewski [35] and Berger [36] that the damping torque in the LLG equation could have a negative sign as well, corresponding to a negative sign of α. This means that the magnetization vector could move into a final position antiparallel to the effective field. In order to achieve this, energy has to be supplied to the FM system to make the angle between the magnetization and the effective field larger. This energy is thought to be provided by the injection of a spin current $\vec{I}^{\text{incident}}$ to the FM [13,32,37]

$$\vec{\tau}^{\text{s}} = -\frac{\gamma}{M_{\text{S}}^2 V}\{\vec{M} \times [\vec{M} \times \vec{I}^{\text{injected}}]\}, \tag{16}$$

which describes the dynamics of a monodomain FM of volume V that is subject to the spin current $\vec{I}^{\text{incident}}$ and modifies the right-hand side of the LLG equation as a source term. In general, a torque term additional to the Slonczewski's torque [Eq. (16)] is also allowed [32,38],

$$\vec{\tau}^{\text{s}\beta} = -\frac{\gamma}{M_{\text{S}} V}\beta[\vec{M} \times \vec{I}^{\text{incident}}], \tag{17}$$

where β gives the relative strength with respect to the Slonczewski's torque [Eq. (16)].

For the case of a FM chain, we assume that the above spin-transfer torques act solely on the last FM cell.

C. Numerical results for interface effects

In order to simulate the enhanced Gilbert damping and the spin-transfer torque, we assume that they act only on the chain end (motivated by their aforementioned origin). So the dynamics of our FM chain is described by the LLG [19,20] equations

$$\begin{aligned}\frac{\partial \vec{M}_n}{\partial t} &= -\frac{\gamma}{1+\alpha^2}\left[\vec{M}_n \times \vec{H}_n^{\text{eff}}\right] \\ &\quad -\frac{\gamma\alpha}{(1+\alpha^2)M_{\text{S}}}\left\{\vec{M}_n \times \left[\vec{M}_n \times \vec{H}_n^{\text{eff}}\right]\right\}, \\ n &= 1, \ldots, (N-1),\end{aligned} \tag{18}$$

and

$$\begin{aligned}\frac{\partial \vec{M}_N}{\partial t} &= -\frac{\gamma}{1+\alpha_N^2}\left[\vec{M}_N \times \vec{H}_N^{\text{eff}}\right] \\ &\quad -\frac{\gamma\alpha_N}{\left(1+\alpha_N^2\right)M_{\text{S}}}\left\{\vec{M}_N \times \left[\vec{M}_N \times \vec{H}_N^{\text{eff}}\right]\right\} \\ &\quad -\frac{\gamma}{M_{\text{S}}^2 a^3}\{\vec{M}_N \times [\vec{M}_N \times \vec{I}^{\text{injected}}]\} \\ &\quad -\frac{\gamma}{M_{\text{S}} a^3}\beta[\vec{M}_N \times \vec{I}^{\text{incident}}],\end{aligned} \tag{19}$$

where $\alpha_N = \alpha + \gamma\hbar g_{\text{eff}}/(4\pi a M_s)$.

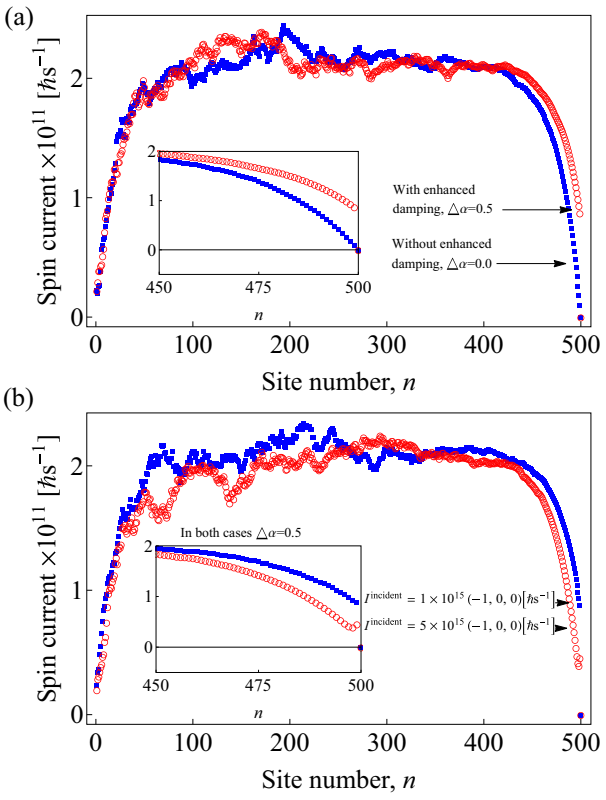

FIG. 10. (Color online) Statistically averaged spin current in the chain of $N = 500$ sites. Numerical parameters are $\Delta T = 100$ K, $\alpha = 0.01$, and $H_0 = 0$ T. The temperature gradient is linear and the maximum temperature is on the left-hand side of the chain (T_1). (a) The blue curve shows the averaged spin current when no enhanced Gilbert damping and no spin-transfer torque is present. The red curve shows the averaged spin current when the enhanced Gilbert damping with $g_{\text{eff}} = 1.14 \times 10^{22}$ m^{-2} is present. The inset shows the averaged spin current of the last 50 sites only. (b) Numerical parameters are $g_{\text{eff}} = 1.14 \times 10^{22}$ m^{-2} and $\beta = 0.01$. The blue curve has $\vec{I}^{\text{incident}} = 1 \times 10^{15}(-1,0,0)$ $\hbar$s^{-1} and the red curve is with $\vec{I}^{\text{incident}} = 5 \times 10^{15}(-1,0,0)$ $\hbar$s^{-1}.

Equations (18) and (19) describe the magnetization dynamics in the presence of the interface effects and include both spin-pump and spin-torque effects. Results in the absence of the spin torque are presented in Fig. 10(a). The enhanced Gilbert damping captures losses of the spin current associated with the interface effect. A nonzero spin current corresponding to the last $n = 200$ spin quantifies the amount of the spin current pumped into the NM from the magnetic insulator. However, the convex profile of the spin current is observed in the presence of the interface effects as well. The influence of the spin torque on the spin-current profile is shown in Fig. 10(b). The most important information from these results is that the large spin torque reduces the total spin current following through the FM-insulator/NM interfaces. The

spin-torque current is directed opposite to the spin-pump current and therefore compensates it.

VII. MECHANISMS OF THE FORMATION OF EXCHANGE SPIN TORQUE AND SPIN-SEEBECK CURRENT

In the previous sections we demonstrated the direct connection between the spin-Seebeck current profile and the exchange spin torque. Here we consider the mechanisms of the formation of the exchange spin torque. For this purpose we investigate changes in the magnetization profile associated with the change of the magnon temperature $\langle \Delta M_n^z \rangle = \langle M_n^z \rangle - \langle M_{0n}^z \rangle$, where $\langle M_n^z \rangle$ is the mean component of the magnetization moment for the case of the applied linear thermal gradient, while $\langle M_{0n}^z \rangle$ corresponds to the mean magnetization component in the absence of thermal gradient $\Delta T = 0$. Quantity $\langle \Delta M_n^z \rangle$ defines the magnon accumulation as the difference between the relative equilibrium magnetization profile and excited one [39] and is depicted in Fig. 11. We observe a direct connection between the magnon accumulation effect and the exchange spin torque. A positive magnon accumulation, meaning an excess of the magnons compared to the equilibrium state is observed in the high-temperature part of the chain. While in the low-temperature part the magnon accumulation is negative, indicating a lack of magnons compared to the equilibrium state. The exchange spin torque is positive in the case of the positive magnon accumulation and is negative in the case of the negative magnon accumulation (the exchange spin torque vanishes in the equilibrium state). From the physical point of view, the result is comprehensible: The spin-Seebeck current is generated by the magnon accumulation, transmitted through the equilibrium part of the chain, and partially absorbed in the part of the chain with a negative magnon accumulation.

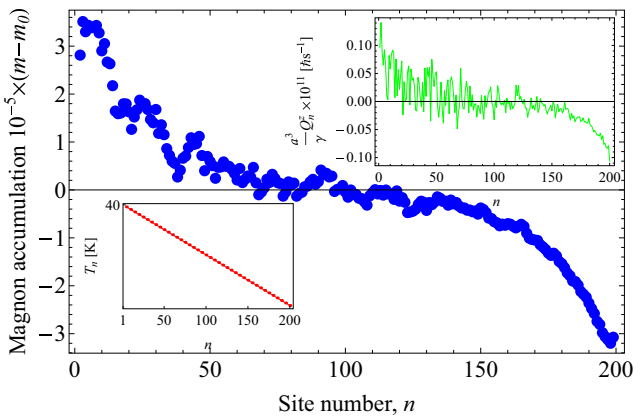

FIG. 11. (Color online) Site dependence of the magnon accumulation effect and the exchange spin torque (top inset) showing a direct connection between the magnon accumulation effect and the exchange spin torque for the given temperature profile (bottom inset). A positive magnon accumulation, i.e., an excess of the magnons, is observed in the high-temperature part of the chain, while in the low-temperature part the magnon accumulation is negative (lack of magnons compare to the equilibrium state). The exchange spin torque is positive for a positive magnon accumulation and negative for a negative magnon accumulation. The spin-Seebeck current is generated by excess magnons, transmitted through the equilibrium part of the chain and partially absorbed in the region with magnon drain.

VIII. INFLUENCE OF FERROMAGNETIC DOMAINS ON THE SPIN CURRENT

Among the various mechanisms/energies governing the magnetism of a material, the exchange interaction is usually dominant with an associated energy typically exceeding the dipole-dipole interaction by at least two orders of magnitude. Since, however, the exchange interaction has a short-range contribution, in FM materials with a length exceeding considerably the exchange length $\sqrt{\mathrm{A}/(\mu_0 \mathrm{M_S^2})}$ the dipole-dipole interaction causes formation of FM domains [22,23]. In order to address this issue in the context of the present work, the methodology of Ref. [40] was employed to enforce the formation of domain walls by implementing boundary conditions such that the magnetization at the chain ends is aligned antiparallel. First, we assured that at $T = 0$ K and $\vec{\nabla} T = 0$ K the ground-state configuration is a FM domain wall of the Bloch type (inset of Fig. 12). When applying a thermal bias to the FM chain, we observe that the domain wall shifts towards the hot edge of the system (Fig. 12). This is because the free energy of the domain wall $\triangle F = \triangle E - T \triangle S$ is a monotonically decaying function of the temperature, where $\triangle E$ is the internal energy density and $\triangle S$ is the entropy density. Thus, the motion of the domain wall to the hot edge minimizes the energy. In addition, we studied the influence of the domain wall on the spin-current profile and found that the total modifications are not significant (Fig. 13). Therefore, we argue that for the sizes of FM chains considered here our statements concerning the magnon accumulation effect, the exchange spin torque, and the formation of the spin current

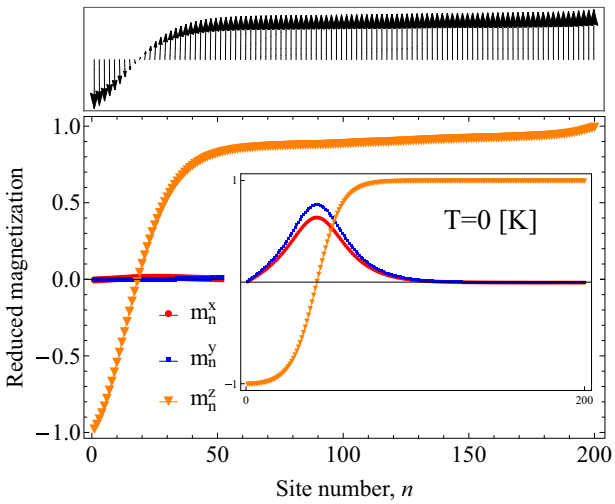

FIG. 12. (Color online) Statistically averaged (1000 times) reduced magnetization configuration (top bar) and its Cartesian components (the graph) as a function of the site number. Numerical parameters are $\Delta T = 40$ K, $\alpha = 0.1$, $a_{\mathrm{FM}} = 1$ nm, and $H_0 = 0$ T. The temperature gradient is linear; the maximum temperature is on the left-hand side of the chain ($T_1 = 40$ K). A domain wall is formed due to the assumption of antiparallel alignment of the magnetization at the ends of the chain. The inset shows $T = 0$ K and $\vec{\nabla} T = 0$ K configuration with no averaging.

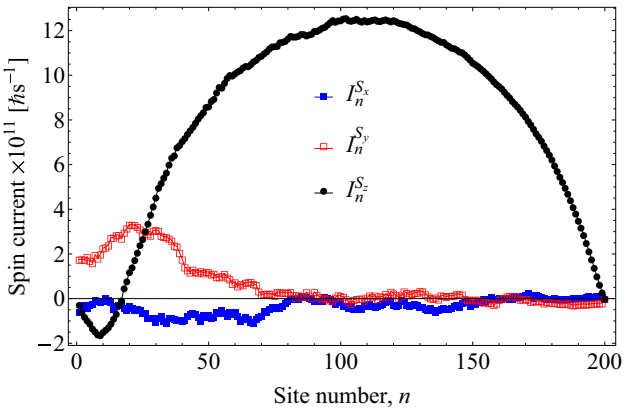

FIG. 13. (Color online) Cartesian components of the statistically averaged longitudinal spin current as a function of the site number for the numerical parameters and the domain wall as in Fig. 12. The spin current is averaged over 1000 realizations.

still hold even in the presence of the dipole-dipole interaction that causes a formation of FM domains.

We finally note that the results for the spin current shown in Fig. 13 can support the hypothesis of the field-dependent spin current reported in Ref. [7] for a mm-sized YIG sample. The authors claim that the scattering of magnons on the domain walls suppresses the spin current at low magnetic fields, which is eliminated upon increasing the magnetic field. As a consequence, there exists a threshold magnetic field above which the spin current rapidly increases. We observe a similar effect in Fig. 13: In the middle of the domain wall the spin current for the chosen geometry changes its sign. As in this experiment, when one applies a sufficiently strong magnetic field, the magnetic configuration changes from the one shown in Fig. 12 to a strictly collinear alignment of the magnetic moments, resulting in a sign-independent and hence a high-net-spin current.

IX. CONCLUSIONS

Based on the solution of the stochastic LLG equation discretized for a chain of FM insulators in the presence of a temperature gradient formed along the chain, we studied the longitudinal SSE with a focus on the space-dependent effects. In particular, we introduced a definition [Eq. (10)] and calculated the longitudinal averaged spin current as a function of different temperature gradients (Fig. 3), temperature gradient strengths (Fig. 5), distinct chain lengths (Fig. 6), and differently oriented external static magnetic fields (Fig. 9). Our particular interest was to explain the mechanisms of the formation of the spin-Seebeck current beyond the linear response regime. The merit was in pointing out a microscopic mechanism for the emergence of the spin-Seebeck current in a finite-size system. In contrast to the macrospin case [14], we obtained a highly nonuniform distribution of the spin current within the FM chain, typically showing a maximum in the middle of the chain (e.g., Figs. 2, 3, and 6). In addition, we have shown that, within our model, the microscopic mechanism of the spin-Seebeck current is the magnon accumulation effect quantified in terms of the exchange spin torque. We proved that the magnon accumulation effect drives the spin-Seebeck current even in the absence of significant deviation between magnon and phonon temperature profiles. Our theoretical findings are in line with recently observed experimental results [18], where nonvanishing spin-Seebeck current was observed in the absence of a temperature difference between phonon and magnon baths.

Concerning the influence of the external constant magnetic fields on the spin-Seebeck current we found that their role is nontrivial: An external static magnetic field applied perpendicularly to the FM chain and along the easy axis may suppress the spin current at elevated magnetic fields [Fig. 9(a)]. The threshold magnetic field has a strength of the anisotropy field, i.e., $2K_1/M_S \sim 0.056$ T. In the case of the magnetic field applied perpendicularly to the easy axis, we observe a more complex behavior [Fig. 9(b)]. In analogy with the situation seen in Fig. 9(a) there are no sizable changes for the $I_{26}(\Delta T)$ dependence at low static fields. This is the regime where the anisotropy field is dominant. In contrast to the H_0^z applied field, it does not linearly depend on the strength of the field [inset of Fig. 9(a)], which is explained by the presence of different competing contributions in the total energy and not a simple correction of the Z component of the anisotropy field. Notably, the magnetic field oriented along the FM chain can also suppress the emergence of the spin current's profile. Also in this case a strong magnetic field destroys the formation of the magnetization gradient resulting from the applied temperature bias.

In addition, we modeled an interface formed by a nonuniformly magnetized finite-size ferromagnetic insulator and a NM (e.g., YIG-platinum junction) to inspect the effects of the enhanced Gilbert damping on the formation of space-dependent spin current within the chain. The results of these simulations (Fig. 10) evidenced a nonvanishing spin current flowing from the FM/NM interface into the NM.

Finally, we studied the influence of the dipole-dipole interaction and domain walls on the formation of the spin current (Figs. 12 and 13). We proved that for the sizes of FM chains considered here, our statements concerning the magnon accumulation effect, the exchange spin torque, and the formation of the spin current still hold even in the presence of the dipole-dipole interaction that causes domain formation.

ACKNOWLEDGMENTS

We gratefully acknowledge fruitful discussions with S. Trimper. This work is supported by the International Max Planck Research School for Science and Technology of Nanostructures. Financial support by the Deutsche Forschungsgemeinschaft (DFG) through SFB 762, Contract No. BE 2161/5-1, is gratefully acknowledged.

[1] K. Uchida, S. Takahashi, K. Harii, J. Ieda, W. Koshibae, K. Ando, S. Maekawa, and E. Saitoh, Nature (London) **455**, 778 (2008).

[2] M. Hatami, G. E. W. Bauer, Q. Zhang, and P. J. Kelly, Phys. Rev. B **79**, 174426 (2009); A. D. Avery, M. R. Pufall, and B. L. Zink, Phys. Rev. Lett. **109**, 196602 (2012); C. H. Wong,

H. T. C. Stoof, and R. A. Duine, Phys. Rev. A **85**, 063613 (2012).

[3] S. Bosu, Y. Sakuraba, K. Uchida, K. Saito, T. Ota, E. Saitoh, and K. Takanashi, Phys. Rev. B **83**, 224401 (2011); C. M. Jaworski, R. C. Myers, E. Johnston-Halperin, and J. P. Heremans, Nature (London) **487**, 210 (2012); D. G. Rothe, E. M. Hankiewicz, B. Trauzettel, and M. Guigou, Phys. Rev. B **86**, 165434 (2012).

[4] C. M. Jaworski, J. Yang, S. Mack, D. D. Awschalom, J. P. Heremans, and R. C. Myers, Nat. Mater. **9**, 898 (2010); A. Slachter, F. L. Bakker, and B. J. van Wees, Phys. Rev. B **84**, 020412(R) (2011); F. K. Dejene, J. Flipse, and B. J. van Wees, *ibid.* **86**, 024436 (2012).

[5] K. Uchida, J. Xiao, H. Adachi, J. Ohe, S. Takahashi, J. Ieda, T. Ota, Y. Kajiwara, H. Umezawa, H. Kawai, G. Bauer, S. Maekawa, and E. Saitoh, Nat. Mater. **9**, 894 (2010).

[6] J. Xiao, G. E. W. Bauer, K.-c. Uchida, E. Saitoh, and S. Maekawa, Phys. Rev. B **81**, 214418 (2010).

[7] K. Uchida, T. Nonaka, T. Ota, H. Nakayama, and E. Saitoh, Appl. Phys. Lett. **97**, 262504 (2010); D. Qu, S. Y. Huang, J. Hu, R. Wu, and C. L. Chien, Phys. Rev. Lett. **110**, 067206 (2013); M. Weiler, H. Huebl, F. S. Goerg, F. D. Czeschka, R. Gross, and S. T. B. Goennenwein, *ibid.* **108**, 176601 (2012); M. R. Sears and W. M. Saslow, Phys. Rev. B **85**, 035446 (2012).

[8] M. Schreier, A. Kamra, M. Weiler, J. Xiao, G. E. W. Bauer, R. Gross, and S. T. B. Goennenwein, Phys. Rev. B **88**, 094410 (2013); N. Roschewsky, M. Schreier, A. Kamra, F. Schade, K. Ganzhorn, S. Meyer, H. Huebl, S. Geprägs, R. Gross, S. T. B. Goennenwein, Appl. Phys. Lett. **104**, 202410 (2014); R. Jansen, A. M. Deac, H. Saito, and S. Yuasa, Phys. Rev. B **85**, 094401 (2012).

[9] J. Torrejon, G. Malinowski, M. Pelloux, R. Weil, A. Thiaville, J. Curiale, D. Lacour, F. Montaigne, and M. Hehn, Phys. Rev. Lett. **109**, 106601 (2012).

[10] N. Li, J. Ren, L. Wang, G. Zhang, P. Hänggi, and B. Li, Rev. Mod. Phys. **84**, 1045 (2012); J. Ren, Phys. Rev. B **88**, 220406(R) (2013); J. Borge, C. Gorini, and R. Raimondi, *ibid.* **87**, 085309 (2013); S. Y. Huang, X. Fan, D. Qu, Y. P. Chen, W. G. Wang, J. Wu, T. Y. Chen, J. Q. Xiao, and C. L. Chien, Phys. Rev. Lett. **109**, 107204 (2012).

[11] C.-L. Jia and J. Berakdar, Phys. Rev. B **83**, 180401R (2011).

[12] H. Adachi, K. Uchida, E. Saitoh, and S. Maekawa, Rep. Prog. Phys. **76**, 036501 (2013).

[13] Y. Tserkovnyak, A. Brataas, and G. E. W. Bauer, Phys. Rev. Lett. **88**, 117601 (2002).

[14] L. Chotorlishvili, Z. Toklikishvili, V. K. Dugaev, J. Barnas, S. Trimper, and J. Berakdar, Phys. Rev. B **88**, 144429 (2013).

[15] I. D. Mayergoyz, G. Bertotti, and C. Serpico, *Nonlinear Magnetization Dynamics in Nanosystems* (Elsevier, Amsterdam, 2009); R. Betzholz, H. Gao, Z. Zhao, and U. Hartmann, Europhys. Lett. **101**, 17005 (2013).

[16] T. Bose and S. Trimper, Phys. Rev. B **81**, 104413 (2010).

[17] S. Hoffman, K. Sato, and Y. Tserkovnyak, Phys. Rev. B **88**, 064408 (2013).

[18] M. Agrawal, V. I. Vasyuchka, A. A. Serga, A. D. Karenowska, G. A. Melkov, and B. Hillebrands, Phys. Rev. Lett. **111**, 107204 (2013).

[19] T. L. Gilbert, Phys. Rev. **100**, 1243 (1955) (abstract only); IEEE Trans. Magn. **40**, 3443 (2004).

[20] L. D. Landau and E. M. Lifshitz, Phys. Z. Sowjetunion **8**, 153 (1935).

[21] W. T. Coffey and Y. P. Kalmykov, J. Appl. Phys. **112**, 121301 (2012).

[22] J. M. D. Coey, *Magnetism and Magnetic Materials* (Cambridge University Press, Cambridge, 2010).

[23] R. C. O'Handley, *Modern Magnetic Materials: Principles and Applications* (Wiley-Interscience, New York, 1999).

[24] T. Kikkawa, K. Uchida, Y. Shiomi, Z. Qiu, D. Hou, D. Tian, H. Nakayama, X.-F. Jin, and E. Saitoh, Phys. Rev. Lett. **110**, 067207 (2013).

[25] A. Kapelrud and A. Brataas, Phys. Rev. Lett. **111**, 097602 (2013).

[26] P. E. Kloeden, *Numerical Solution of SDE Through Computer Experiments* (Springer Science & Business Media, Berlin, 1994).

[27] N. G. van Kampen (ed.), *Stochastic Processes in Physics and Chemistry* (Elsevier, Amsterdam, 2007).

[28] A. Sukhov and J. Berakdar, J. Phys.: Condens. Matter **20**, 125226 (2008).

[29] We note that one should properly rescale the magnon-magnon and the magnon-phonon relaxation times given in Ref. [5], since we use in the numerical calculations the optimized values for damping. It is shown in Ref. [6] that the relaxation times are inversely proportional to the magnetization damping.

[30] E. Saitoh, M. Ueda, H. Miyajima, and G. Tatara, Appl. Phys. Lett. **88**, 182509 (2006).

[31] Y. Kajiwara, K. Harii, S. Takahashi, J. Ohe, K. Uchida, M. Mizuguchi, H. Umezawa, H. Kawai, K. Ando, K. Takanashi, S. Maekawa, and E. Saitoh, Nature (London) **464**, 262 (2010).

[32] A. Brataas, A. D. Kent, and H. Ohno, Nat. Mater. **11**, 372 (2012).

[33] X. Jia, K. Liu, K. Xia, and G. E. W. Bauer, Europhys. Lett. **96**, 17005 (2011).

[34] Y. Tserkovnyak, A. Brataas, G. E. Bauer, and B. I. Halperin, Rev. Mod. Phys. **77**, 1375 (2005).

[35] J. C. Slonczewski, J. Magn. Magn. Mater. **159**, L1 (1996).

[36] L. Berger, Phys. Rev. B **54**, 9353 (1996).

[37] L. Chotorlishvili, Z. Toklikishvili, A. Sukhov, P. P. Horley, V. K. Dugaev, V. R. Vieira, S. Trimper, and J. Berakdar, J. Appl. Phys. **114**, 123906 (2013).

[38] J. Stöhr and H. C. Siegmann, *Magnetism: From Fundamentals to Nanoscale Dynamics* (Springer Science & Business Media, Berlin, 2007).

[39] U. Ritzmann, D. Hinzke, and U. Nowak, Phys. Rev. B. **89**, 024409 (2014).

[40] D. Hinzke and U. Nowak, Phys. Rev. Lett. **107**, 027205 (2011); D. Hinzke, N. Kazantseva, U. Nowak, O. N. Mryasov, P. Asselin, and R. W. Chantrell, Phys. Rev. B **77**, 094407 (2008).